

Supporting Information:

Minimal numerical ingredients describe chemical microswimmers' 3-D motion

Maximilian R. Bailey,^{a,b} C. Miguel Barriuso Gutiérrez,^b José Martín-Roca,^{b,c}

Vincent Niggel,^a Virginia Carrasco-Fadanelli,^d Ivo Buttinoni,^d

Ignacio Pagonabarraga,^{e,f} Lucio Isa,^a and Chantal Valeriani^{b,g,*}

^aLaboratory for Soft Materials and Interfaces, Department of Materials

ETH Zürich, Zürich, Switzerland

^bDepartamento de Estructura de la Materia, Física Térmica y Electrónica,

Universidad Complutense de Madrid, Madrid, Spain

^cDepartamento de Química Física, Facultad de Química,

Universidad Complutense de Madrid, Madrid, Spain

^dDepartment of Physics, Institute of Experimental Colloidal Physics,

Heinrich-Heine University, Düsseldorf, Germany

^eDepartament de Física de la Matèria Condensada,

Universitat de Barcelona, Barcelona, Spain

^fUniversitat de Barcelona Institute of Complex Systems (UBICS),

Universitat de Barcelona, Barcelona, Spain

^gGISC - Grupo Interdisciplinar de Sistemas Complejos

Madrid, Spain

*To whom correspondence should be addressed: *

E-mail: cvaleriani@ucm.es

The Supporting Information includes:

Fig. S1: Sedimentation of passive colloids under gravity

Fig. S2: Trajectory of a microswimmer which leaves the plane

Fig. S3: Velocity Distributions binned by different definitions of swimming direction

Fig. S4: Effect of thermal noise on the dynamics of a microswimmer without shape asymmetry

Fig. S5: Rendering of different shape asymmetries (1 Edge, 1 Centre, 2 Edges)

Fig. S6: Role of shape asymmetry on the dynamics of a microswimmer (1 Edge case)

Fig. S7: Role of shape asymmetry on the dynamics of a microswimmer (1 Centre case)

Fig. S8: Role of shape asymmetry on the dynamics of a microswimmer (2 Edges case)

Fig. S9: Periodic boundary conditions and finite size effects

Fig. S10: XY slices of the flow fields generated by microswimmers in the laboratory frame

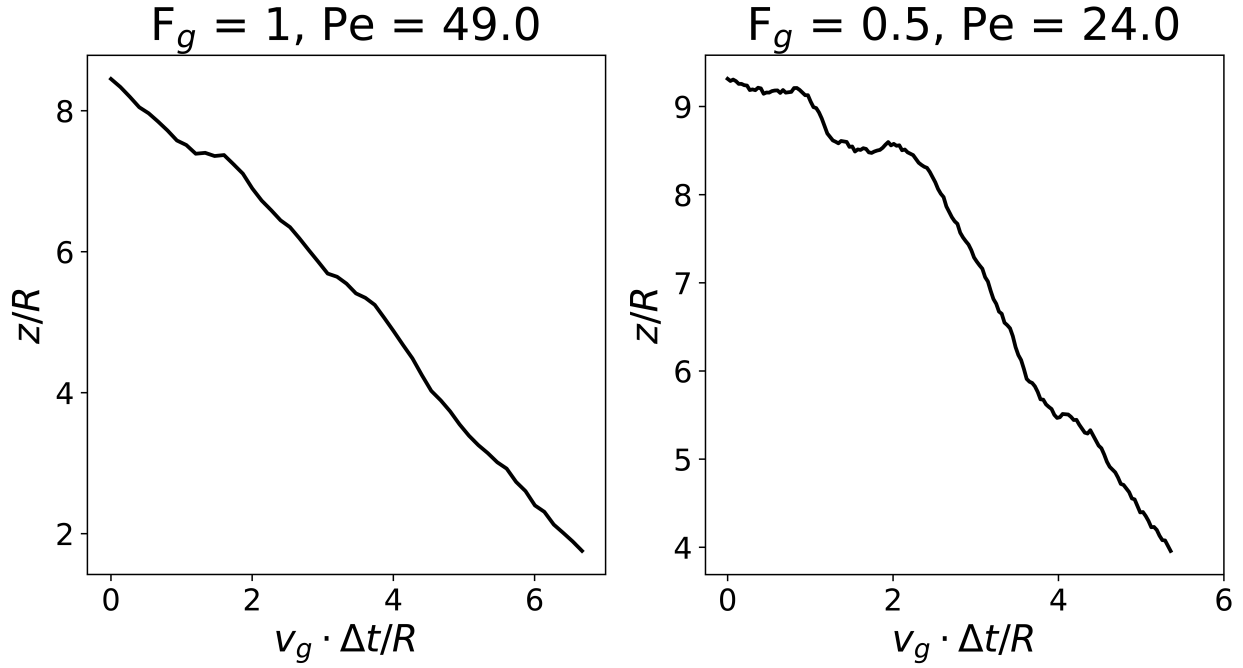


Figure. S 1: Verification of the solvent parameters used to ensure a low Re regime. The gravitational force F_g applied to a sedimenting colloid is halved (from $F_g = 1$ to $F_g = 0.5$, left panel and right panel respectively), with the corresponding reduction in sedimentation velocity and thus Péclet number ($Pe = v_g * R/D_T$, where v_g is the velocity due to gravity, and R, D_T are constant properties of the colloid) - as expected by Stokes law. We note that the forces involved are relatively low when $F_g = 0.5$, leading to increasingly important role of Brownian fluctuations. As the gravitational force is increased further, dz/dt will become increasingly linear (as Pe increases).

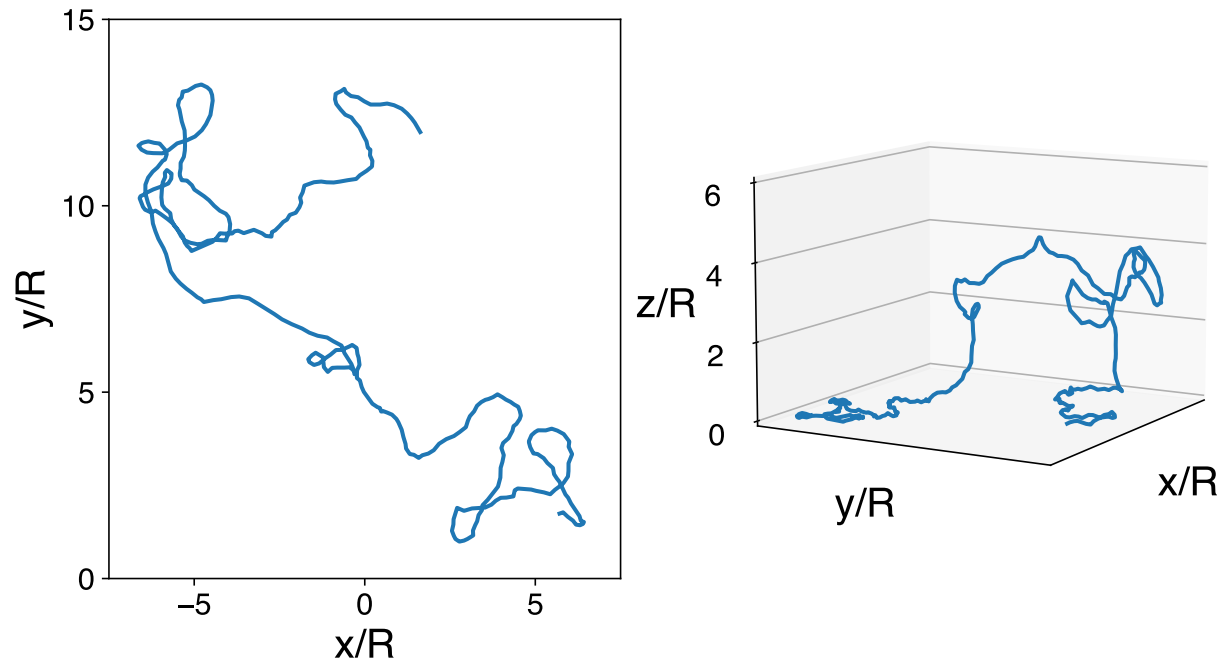


Figure. S 2: An example trajectory of the 3-D motion of a microswimmer (right panel), with its 2-D projection onto the XY plane (left panel). We note that particle motion is characterised by long periods of motion in the 2-D plane, interspersed with out-of-plane (z) loops.

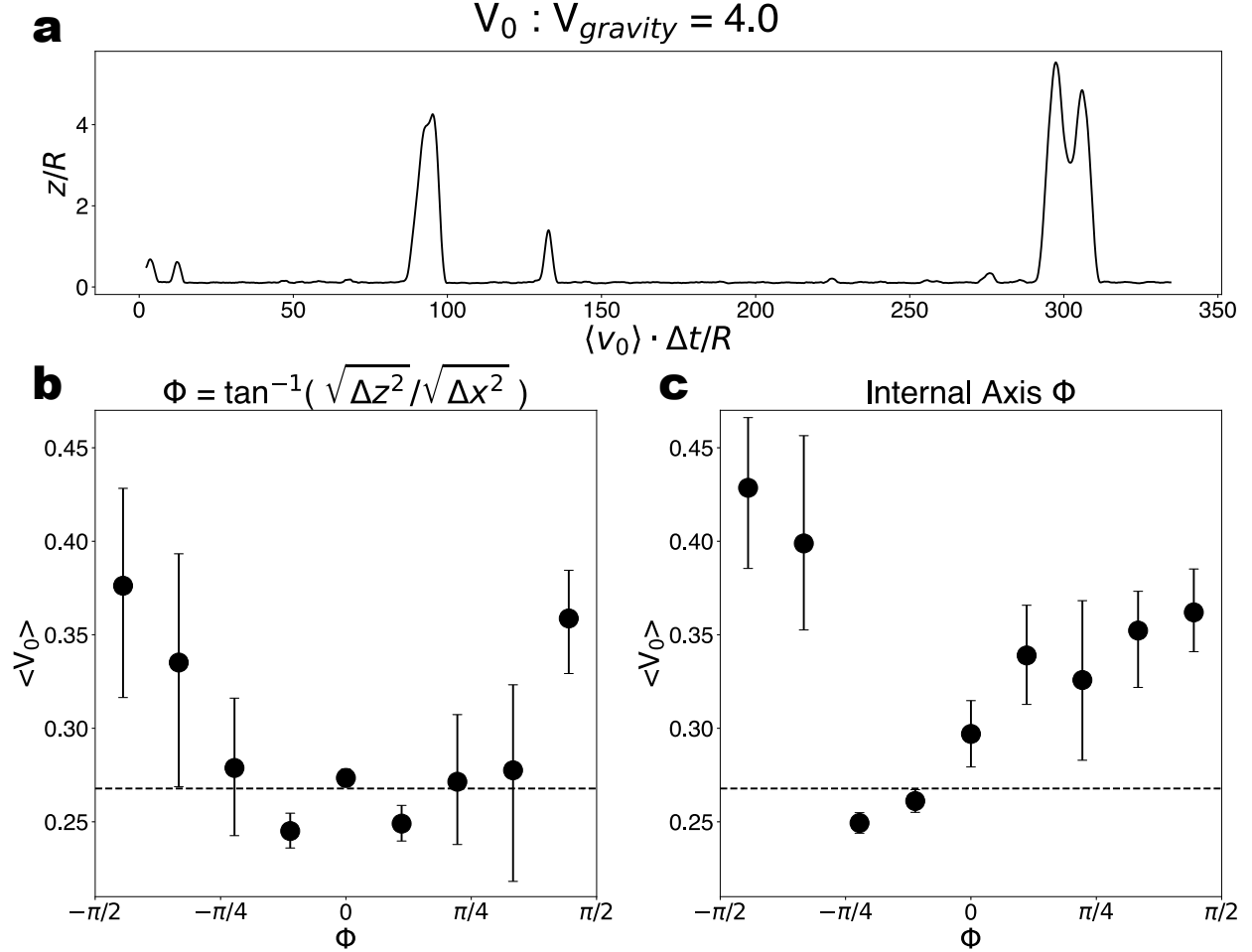


Figure. S 3: a) The out-of-plane trajectory of a simulated CB microswimmer ($z(t)$). b) Using the analysis proposed in,^{1,2} i.e. binning the instantaneous displacements of the microswimmer by the zenith angle calculated from those displacements, results in the same data structure as that found experimentally.^{1,2} This suggests that the “orientation-dependent velocity” previously reported is in fact an inherent feature of the analytical approach used, rather than arising from e.g. the microswimmers’ photo-responsiveness. c) Analysing the data using the internal orientation axis (known in simulations), we recover a more explainable structure. Specifically, when the particle swims down from the bulk towards the substrate ($-\pi/2 < \Phi < -\pi/4$), it obtains the expected boost in velocity due to gravity. For $-\pi/4 < \Phi < 0$, the velocities are significantly lower, as this corresponds to the region where the particle is at the substrate and facing towards it due to hydrodynamic attraction (see Figure 2 h.). The particle speed here is lower as it only consists of the projection of the velocity onto the substrate. We note that this corresponds to the largest part of the trajectory, significantly reducing the overall average velocity (dashed line). As the particle leaves the substrate ($0 < \Phi$), the particle swims faster than at the substrate, but as it swims against gravity is not as fast as for $-\pi/2 < \Phi < -\pi/4$. These results suggest that coarse-graining the effect of phoretic and light fields to hydrodynamic interactions and gravity is indeed sufficient to capture the physics of various experimental chemical microswimmer systems.

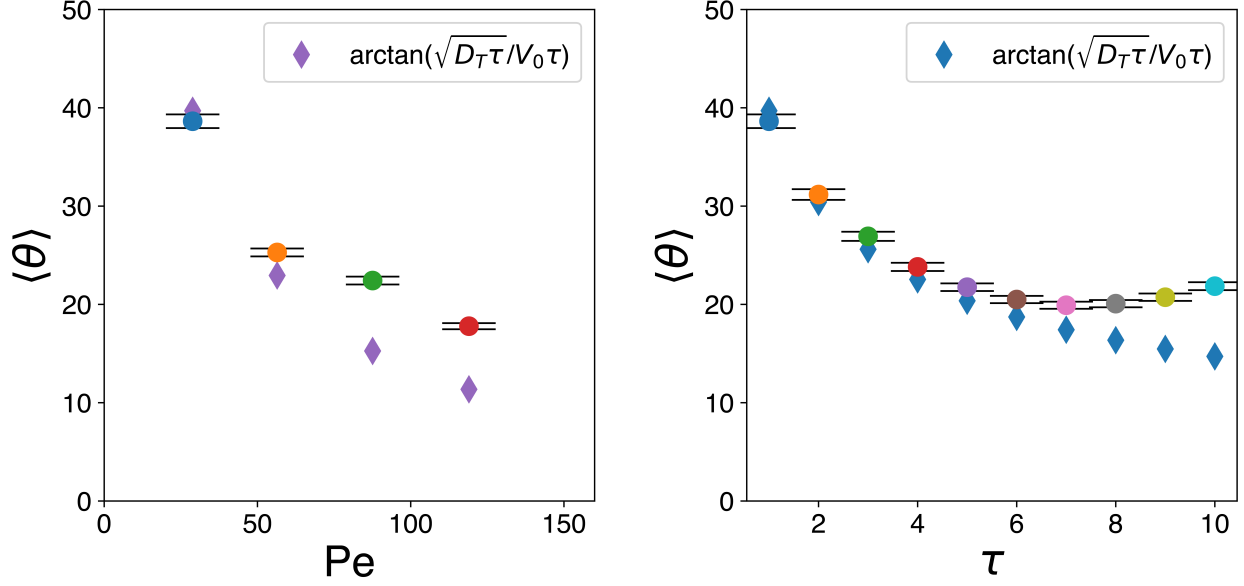


Figure. S 4: Investigation of the angle θ between the swimming direction and internal orientation (defined by the body axis) of our microswimmers in bulk and in the absence of any shape asymmetry ($R_{shift} = 0$). Left panel: The change in θ as the swimming velocity of the microswimmer is increased (represented via $Pe = v_p \cdot R/D_T$). Right panel: The change in θ as the lag-time τ over which the subsequent displacements are evaluated (see main text for discussion of definitions). In both cases, the diamonds represent the values estimated if assuming translational diffusion occurs only perpendicular to the internal swimming axis. As no gravitational force nor substrate is present, one may expect that the internal orientation and swimming direction of a weak pusher squirmer would align perfectly. However, from our analysis we find that this is not the case. We propose that thermal fluctuations, namely rotational and translational diffusion of the particle, are the key contributing factors to this observation. On the left, we see that at lower Pe numbers, the significant divergence between the swimming direction and internal orientation can be completely explained by the expected translational diffusion of the particle. We find that as the Pe is increased, both the observed and theoretical θ between the two vectors follow the same trend, in that the value of $\langle \theta \rangle$ decreases. We also see on the right that by increasing lag time over which the displacements are evaluated, the observed and expected $\langle \theta \rangle$ values also become smaller. This points to the role of the microswimmer's diffusivity in defining its motion, and thus the angle between the swimming direction and the body axis in the case of $R_{shift} = 0$ (no shape asymmetry). Due to finite time differencing, we also expect the rotational diffusivity of the squirmer to play a further role in the difference between the particles internal orientation and swimming displacement in bulk. For example, we take the average of the particle's internal orientation between two time steps, which will introduce a component of noise due to rotational diffusion between those steps. We also expect these effects to contribute to the saturation of the effect of shape asymmetry at $\theta \sim 35^\circ$.

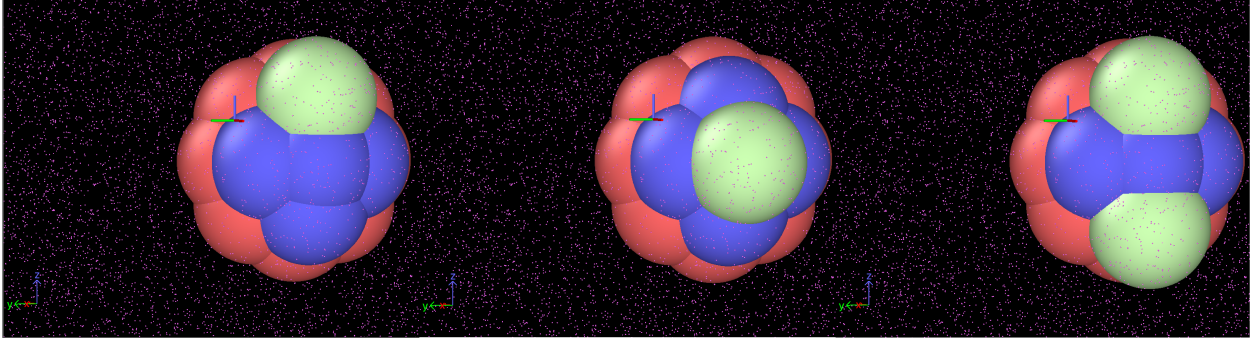


Figure. S 5: Overview of the different types of shape asymmetry introduced via shape particles P_s with $R_{shift} = 0.5$ (light green) along the axes of different “cap” particles (blue) for CF microswimmers. Left panel: “1 Edge” case, where P_s is introduced at a 45° angle to the internal body axis (central blue particle). Middle panel: “1 Centre” case, where P_s is introduced along the internal body axis. Right panel: “2 Edge” case, where the two P_s particles are introduced at 45° and -45° to the internal body axis (central blue particle). In all cases, the swimming direction is with the blue cap pointing forwards. The red particles are the remaining “filler” particles constituting the rest of the microswimmer body. Solvent particles are reduced for scale and represented in purple. Graphics were generated using the visualisation software Ovito³

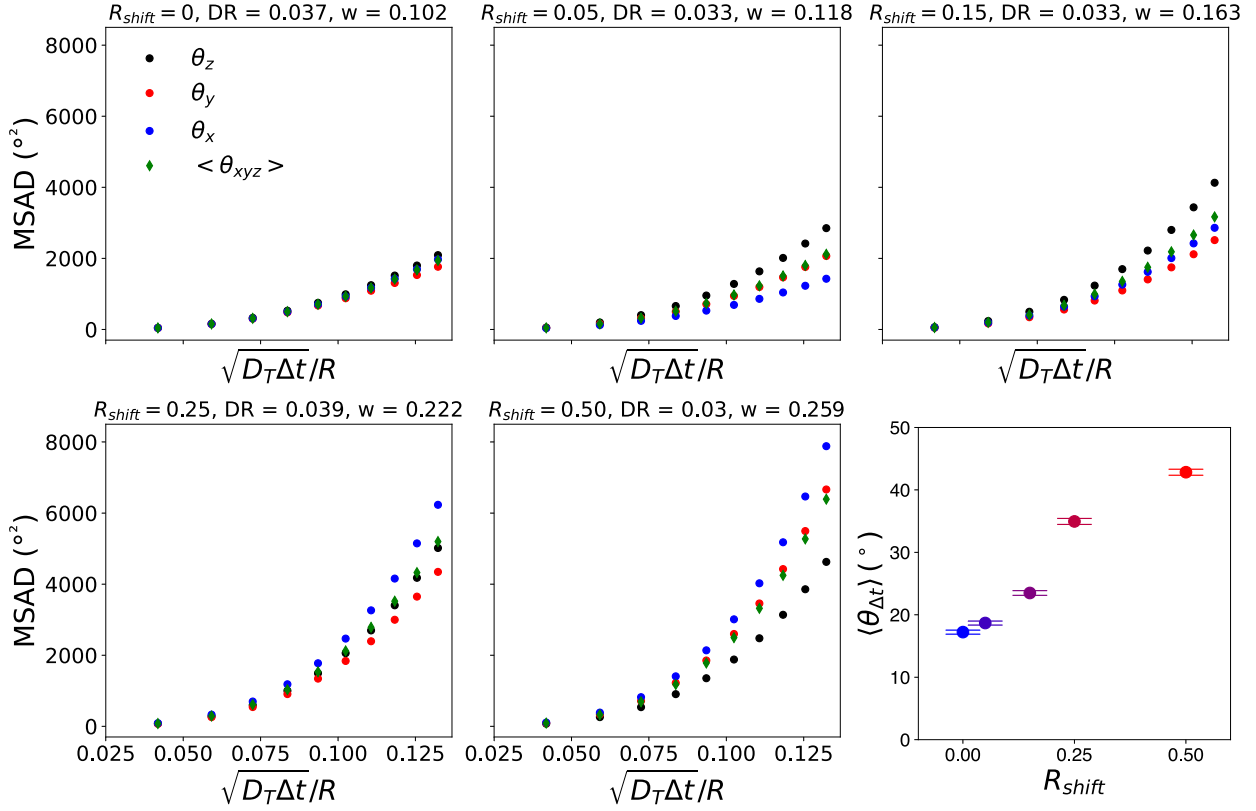


Figure. S 6: MSADs for the simulated bulk microswimmers for increasing values of R_{shift} for the “1 Edge” case, as described in Figure S5. The calculated angles between the swimming direction and internal orientation of bulk microswimmers, also discussed in Figure 4 of the main text, are shown in the bottom right panel. Error bars indicate the standard error of the mean from 1001 frames (sub-sampled from 50000 simulation steps).

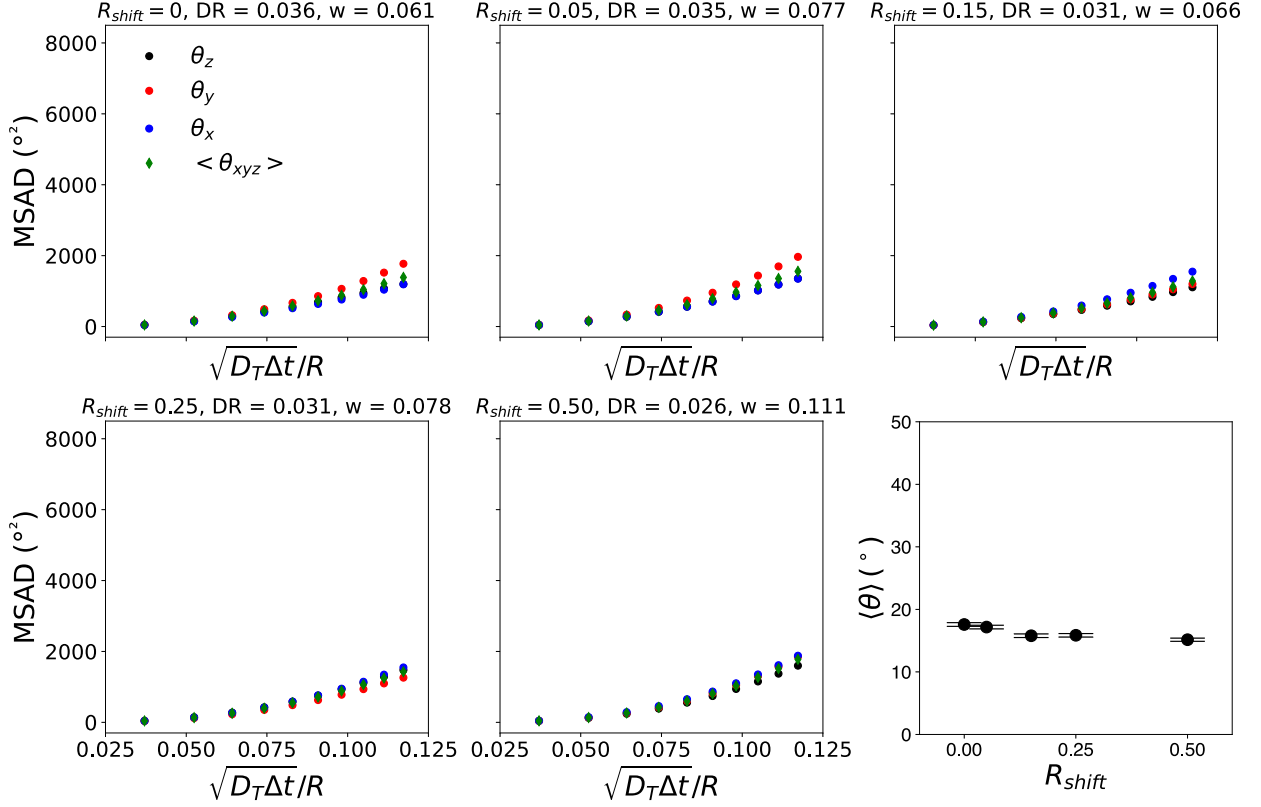


Figure. S 7: MSADs for the simulated bulk microswimmers for increasing values of R_{shift} for the “1 Centre” case, as described in Figure S5. The calculated angles between the swimming direction and internal orientation of bulk microswimmers are shown in the bottom right panel. We note that the reduced asymmetry introduced by a P_{shape} particle along the internal microswimmer orientation has little effect on its dynamics, contrasting to the “1 Edge” case. Error bars indicate the standard error of the mean from 1001 frames (sub-sampled from 50000 simulation steps).

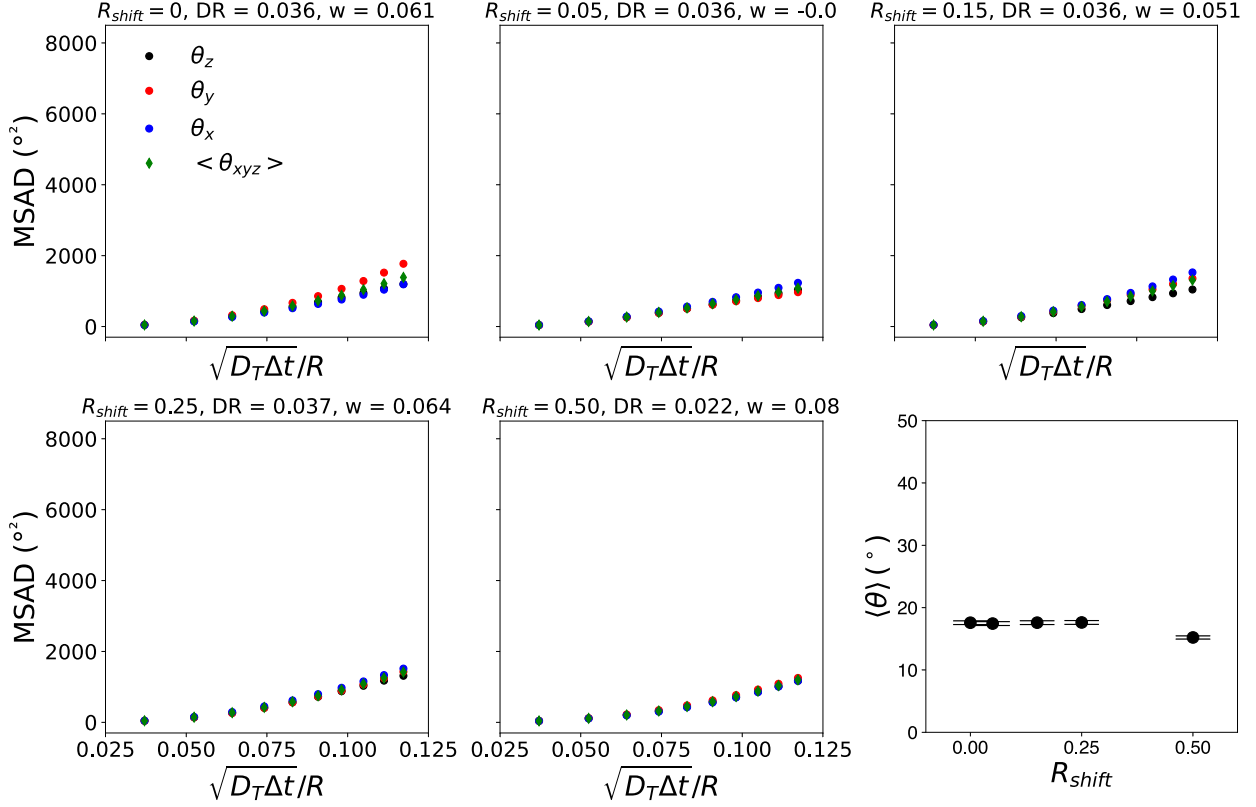


Figure. S 8: MSADs for the simulated bulk microswimmers for increasing values of R_{shift} for the “2 Edge” case, as described in Figure S5. The calculated angles between the swimming direction and internal orientation of bulk microswimmers are shown in the bottom right panel. We note that the reduced asymmetry introduced by 2 P_{shape} particles on the edges of the microswimmer, resulting in mirror symmetry along its internal orientation axis, has little effect on the swimming dynamics, contrasting to the “1 Edge” case. This is despite the introduction of 2 P_{shape} particles on positions each corresponding to the “1 Edge” case (opposite each other). This underlines the importance of the overall shape asymmetry of the microswimmer to its physics. Error bars indicate the standard error of the mean from 1001 frames (sub-sampled from 50000 simulation steps).

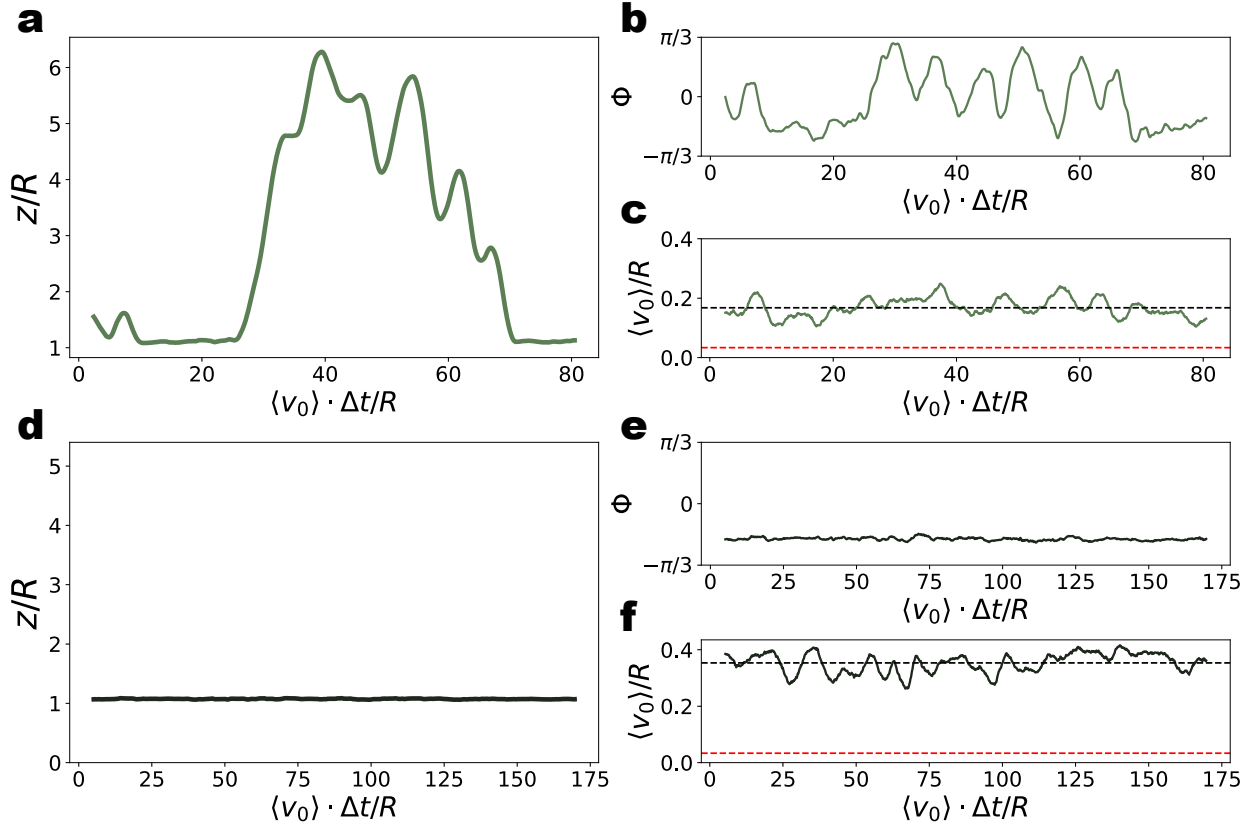


Figure. S 9: As for any simulation method that accounts for hydrodynamics, periodic boundary conditions (PBCs) introduce a finite size effect in the results, which will deviate from analytic predictions for an infinite system. The Péclet number (Pe) quantifies the relevance of self-propulsion against diffusion. At small Pe we do not expect any significant flow profile, while the flow generated by propulsion and stresslets will be developed at high Pe . The DPD model recovers this behavior and generates flow profiles with the symmetries corresponding to the active motion of the microswimmer,⁴ and finite size only affects the quantitative details of the far field hydrodynamic field. To verify that boundary effects do not qualitatively affect our key findings, we re-simulate two situations studied in Figure 3 of (a-c: $Pe = 30$, d-f: $Pe = 100$). Specifically, we increase the system size by 4x (i.e. double the dimensionality in X and Y to be 32x32x40) for these two instances, and investigate whether we observe qualitatively similar behavior (i.e. for $Pe = 100$, the particle cannot leave the substrate, whereas for $Pe = 30$ it can). We observe an almost identical behavior for the significantly larger system as that described in Figure 3, justifying our use of a smaller simulation box to reduce computational expense.

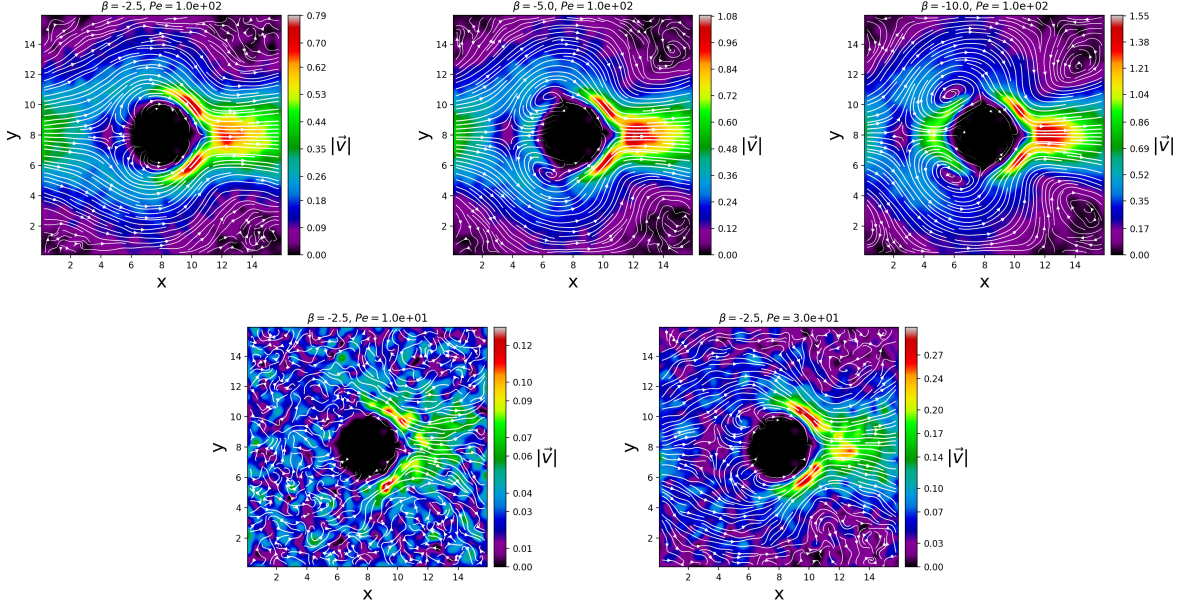


Figure. S 10: XY slices of the flow fields generated by microswimmers in the laboratory frame (through the equator of the particle). **Top row:** Flow fields for fixed $Pe = 100$ and decreasing $\beta = \{-2.5, -5, -10\}$ to increase the *pusher* character of the squirmer. **Bottom row:** Using a fixed value of $\beta = -2.5$ and varying $Pe = \{10, 30\}$, reproducing the findings in Figure 3 of the main text. As the β parameter becomes more negative, we observe the transition from a weak pusher flow field (more reminiscent of a neutral squirmer) to a strong pusher, with the development of the characteristic vortices associated with hydrodynamic pushers. These vortices retain the qualitative shape of a pusher squirmer in periodic boundary conditions with the four characteristic vortices and the saddle point, comparable to those reported previously for squirmers using other numerical schemes.^{5,6} We note that some distortions to the flow field are noticeable due to the idiosyncrasies of the simulation (periodic boundary conditions (PBCs), the presence of the substrate, and the fact that the squirmer is being held fixed with respect to the substrate). In the absence of a gravitational force, the flow field generated by the squirmer is force free, and the main features of this class of flows are preserved irrespective of the system size. It is true that the measured flow field is affected by the flows induced by the periodic images. The magnitude of this contribution will decay with system size, and they can modify details of the flow field, but not the main features of the broken symmetry of the flow field with respect to the direction of motion of the squirmer. In our simulations the squirmer displaces in the presence of a gravitational force. This generates a Stokeslet that also contributes to the shape of the flow field (this feature is also affected by the periodic images and by the presence of the bounding walls). Nevertheless, as discussed in Figure S9, the PBCs do not affect the qualitative features of our findings. Furthermore, we note that for the lower Pe numbers primarily studied in the main text, the effect of the PBCs used are reduced.

References

- (1) Bailey, M. R.; Grillo, F.; Spencer, N. D.; Isa, L. Microswimmers from Toposelective Nanoparticle Attachment. *Advanced Functional Materials* **2022**, *32*, 2109175.
- (2) Bailey, M. R.; Gmür, T. A.; Grillo, F.; Isa, L. Modular Attachment of Nanoparticles on Microparticle Supports via Multifunctional Polymers. *Chemistry of Materials* **2023**, *35*, 3731–3741.
- (3) Stukowski, A. Visualization and analysis of atomistic simulation data with OVITO—the Open Visualization Tool. *Modelling and Simulation in Materials Science and Engineering* **2010**, *18*, 015012.
- (4) Barriuso Gutiérrez, C. M.; Martín-Roca, J.; Bianco, V.; Pagonabarraga, I.; Valeriani, C. Simulating Microswimmers Under Confinement With Dissipative Particle (Hydro) Dynamics. *Frontiers in Physics* **2022**, *10*, 926609.
- (5) Kuron, M.; Stärk, P.; Burkard, C.; de Graaf, J.; Holm, C. A lattice Boltzmann model for squirmers. *The Journal of Chemical Physics* **2019**, *150*, 144110.
- (6) Zöttl, A.; Stark, H. Simulating squirmers with multiparticle collision dynamics. *The European Physical Journal E* **2018**, *41*, 61.